PAPER

Check for updates

A doping-adsorption-pyrolysis strategy for constructing atomically dispersed cobalt sites anchored on a N-doped carbon framework as an efficient bifunctional electrocatalyst for hydrogen evolution and oxygen reduction†

Yuan Pan, [ID] *[ab] Minmin Wang[b] and Chao Feng*[b]

Renewable energy technology development focuses on the exploration of economical and efficient non-precious metal catalysts to replace precious metal catalysts in electrocatalytic reactions including oxygen reduction (ORR) and hydrogen evolution (HER). Herein, we synthesized a cobalt single atom catalyst anchored on a N-doped carbon framework by a doping-adsorption-pyrolysis strategy. The optimized Co SAs/CN-3 catalyst showed excellent HER and ORR bifunctional electrocatalytic performance, which could be attributed to the highly dispersed Co$-N_4$ active sites, large specific surface area and abundant pore structure. Density functional theory shows that the isolated active Co$-N_4$ site shows low hydrogen adsorption Gibbs free energy, and promotes the adsorption of H and oxygen-containing intermediates in HER and ORR. This work not only provides a new idea for the construction of transition metal catalysts with atomic accuracy but also provides powerful guidance for the development of efficient bifunctional electrocatalysts.

Introduction

Hydrogen evolution reactions (HER) and oxygen reduction reactions (ORR) are important in energy conversion processes such as electrocatalytic water splitting, fuel cells, and metal–air batteries, and are essential to facilitate the transition to an environmentally friendly society.[1–4] What hinders the development of commercial applications for HER and ORR is their slow kinetics, which still requires precious metals such as Pt, Ru, and Ir as catalysts for efficient conversion.[5–10] However, noble metal catalysts have inevitable disadvantages: high cost, scarcity, and poor long-term durability. Therefore, it is very important to develop non-noble metal catalysts with low price, high activity and high stability to improve the development of HER and ORR.

In recent years, single-atom catalysts (SACs) have attracted extensive attention because of their maximum utilization of metal atoms and high catalytic activity, among which the Co–N–C catalyst has become one of the most promising alternatives to noble metal catalysts.[11–16] Liu *et al.*[17] reported the origin of Co

SAC activity in HER by combining experimental and theoretical calculations. The density functional theory (DFT) calculation results show that Co SAs located at the edge of graphene are the highly active sites of HER. Zhang *et al.*[18] anchored single Co atoms on hollow carbon spheres co-doped with N and S as an efficient and multi-functional SAC. Experimental characterizations and theoretical mechanism studies revealed that the synergistic effect between atomically dispersed Co–N_4 active sites and nearby electron donor S significantly reduced the potential barrier of the electrocatalytic reaction and improved the reaction activity. However, currently reported Co SACs still existing low intrinsic activity and the number of active sites, and most of them are single-functional catalysts. The bifunctional Co SACs with both high HER and ORR performance is rarely reported. Besides, due to the easy agglomeration of single atoms, the preparation of single atoms catalysts with high loading is difficult to achieve. There are still some challenges in the macroscopic synthesis of single atoms catalysts. Therefore, developing efficient synthesis methods is still a challenge in current research.

In this paper, a nitrogen-doped carbon Co single atoms catalyst (Co SAs/CN-3) with a high specific surface area (846 m^2 g^{-1}) was prepared by doping-adsorption-pyrolysis method using metal–organic framework derivatives as precursors. The stable Co–N_4 single atom coordination structure was determined by aberration-corrected high-angle annular dark-field scanning transmission electron microscopy (AC-HAADF-STEM) and X-ray

[a]Engineering Research Center for Waste Oil Recovery Technology and Equipment, Ministry of Education, Chongqing Technology and Business University, Chongqing 400067, China. E-mail: panyuan@upc.edu.cn; fch_upc@163.com

[b]State Key Laboratory of Heavy Oil Processing, China University of Petroleum (East China), Qingdao 266580, Shandong, China

† Electronic supplementary information (ESI) available. See https://doi.org/10.1039/d2ra03351h

absorption spectroscopy (XAS). DFT results show that the isolated Co–N$_4$ active site shows low Gibbs free energy, and promotes the adsorption of H and oxygen-containing intermediates in HER and ORR. The Co SAs/CN-3 catalyst showed excellent HER and ORR bifunctional electrocatalytic performance. In this paper, we provide an efficient bifunctional catalyst and a research idea for the design and synthesis of SACs.

Results and discussion

As shown in Fig. 1a, we developed a novel doping-adsorption-pyrolysis method to synthesize Co single atom catalyst. Firstly, Co^{2+} is introduced in the preparation of ZIF-8. Since Co^{2+} and Zn^{2+} have a similar atomic radius and the same chemical state, Co^{2+} can occupy the position of Zn^{2+} and construct the mixed binary ZIF-8 structure (ZnCo@ZIF-8). Zn can act as a steric hindrance and effectively avoid the aggregation of Co atoms. Then, a layer of tetrapenylporphyrin cobalt molecules was adsorbed on the surface of ZnCo@ZIF-8 by π–π conjugation to increase the cobalt load. Finally, ZIF-8 was carbonized to form a nitrogen-doped carbon skeleton through high-temperature pyrolysis. Zn volatilizes at high temperature, and Co atoms are anchored by N atoms to obtain Co single atom catalyst with a stable Co–N$_4$ coordination structure (Co SAs/CN-3).
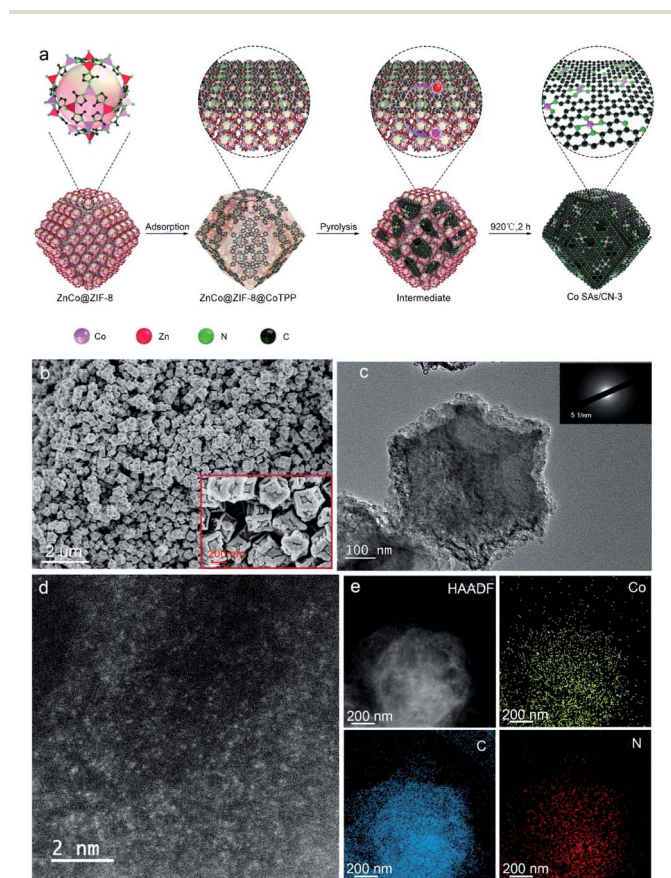

Fig. 1 (a) Schematic illustration of the synthesis process of Co SAs/CN-3, (b) SEM, (c) TEM (the inset is SAED image), (d) AC-HAADF-STEM, (e) HAADF-STEM and EDS mapping.

X-ray powder diffraction patterns (XRD) showed wide peaks at ∼25° and ∼44° respectively, indicating the formation of graphite-carbon structure and high dispersion of Co atoms (Fig. S1†).[19,20] Inductively coupled plasma mass spectrometry (ICP-OES) results showed that Co loading in Co SAs/CN-3 reached 1.03 wt%, which was much higher than that of Co SAs/CN-1 prepared by first doping (0.37 wt%). The above shows that the doping-adsorption-pyrolysis method can effectively improve the metal loading. TEM and SEM images showed that the prepared Co SAs/CN-3 retained the rhombohedron shape and size of the ZIF-8 precursor without obvious particles (Fig. 1b and c). The selected area electron diffraction (SAED) diagram shows that the crystallinity of Co SAs/CN-3 catalyst is poor. In the high-resolution TEM image, there are only lattice stripes of C, but no lattice stripes of Co, indicating that Co atoms are highly dispersed (Fig. S2†). Many isolated bright spots can be observed in the aberration-corrected high-angle annular dark-field scanning transmission electron microscopy (AC-HAADF-STEM) of Co SAs/CN-3 catalyst, indicating that Co disperses uniformly in the form of single atoms (Fig. 1d). EDS mapping shows that Co, N and C atoms are evenly distributed (Fig. 1e).

The X-ray photoelectron spectroscopy (XPS) results confirm the existence of C, N, and Co in the Co SAs/CN-3 catalyst. The peak at 780.1 eV and 795.5 eV in Co 2p spectrum of Co SAs/CN-3 is assigned to Co^{2+} (Fig. S3a†).[21] The XPS spectrum of N 1s is divided into four peaks, corresponding to pyridinic N (398.5 eV), Co–N (399.5 eV), pyrrolic N (400.2 eV) and graphitic N (401.6 eV), respectively (Fig. S3b†).[21] The presence of nitrogen species provides abundant anchoring sites for Co single atoms. The spectrum of C 1s XPS is divided into three peaks with different binding energies, corresponding to the characteristic peaks of C–N (288.1 eV), C=N (285.5 eV) and C=C (284.3 eV), respectively (Fig. S3c†).[22,23]

The pore structure and surface area of Co SAs/CN-3 and Co SAs/CN-1 were analyzed by the N$_2$ adsorption/desorption (Fig. S4 and S5†). The N$_2$ adsorption/desorption curve of Co SAs/CN-3 belongs to the type IV isotherm, indicating abundant pore structure. Co SAs/CN-3 has the highest BET surface area, up to 846 m^2 g^{-1}, which is higher than that of Co SAs/CN-1 (314 m^2 g^{-1}). In addition, Co SAs/CN-1 and Co SAs/CN-3 have a pore volume of 0.07 and 0.36 cm^3 g^{-1} and average pore size of 1.78 and 1.67 nm, respectively. The above results indicate that the doping-adsorption-pyrolysis method can improve the BET surface area of catalysts and expose more active sites. Raman spectra also confirmed that the I_D/I_G value of Co SAs/CN-3 catalyst is 1.23, which is significantly higher than that of Co SAs/CN-1 catalyst (1.02), indicating the abundant defects of the Co SAs/CN-3 catalyst. The highly dispersed porous structure can improve catalytic efficiency by facilitating mass transfer between reactants and products.[24]

The local environment and electronic structure of Co were further studied by X-ray absorption near edge structure (XANES) and extended X-ray absorption fine structure spectrum (EXAFS) (Fig. 3).[25–28] The position of K-edge of Co SAs/CN-3 shows that the Co atom has a positive valence, and its valence state is between 0 and +3 (Fig. 2a). The FT k^3 weighted EXAFS spectrum of Co SAs/CN-3 catalyst has a main peak at 1.5 Å, belonging to
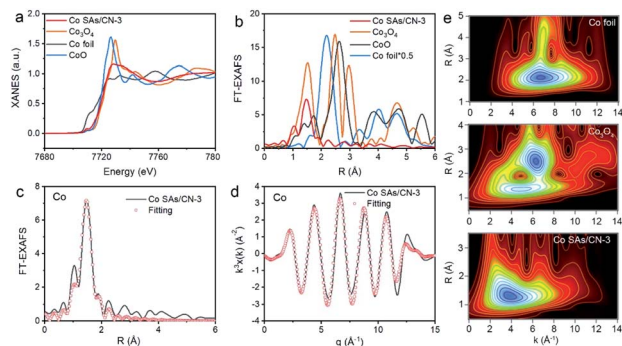
Fig. 2 (a) XANES of Co K-edge, (b) Fourier transform (FT) spectra, EXAFS fitting (c) in R space, (d) in q space, (e) WT contour plots.

the Co–N coordination, and no Co–Co bond is found at 2.2 Å, indicating that Co is single atomically dispersed (Fig. 2b). The wavelet transform of Co SAs/CN-3 only has a maximum intensity at 4 Å^{-1}, corresponding to the Co–N coordination, which further proves that Co is single-atomic dispersed in Co SAs/CN-3 catalyst (Fig. 3e). By EXAFS fitting, the Co–N coordination of Co SAs/CN-3 catalyst is 4 (Fig. 3c and d).

The Co SAs/CN-3 catalyst obtained through a series of optimization experiments has the best electrocatalytic performance of HER (Fig. S6†). When the current density is 10 mA cm^{-2}, Co SAs/CN-3 catalyst needs overpotentials of 238 and 278 mV in 0.5 M H$_2$SO$_4$ and 1 M KOH, respectively, which are lower than that of Co SAs/CN-1 catalyst (810 and 568 mV) (Fig. 3a and d). As shown in Fig. 3b and e, Co SAs/CN-3 catalyst has the lowest Tafel slope of 89.8 mV dec^{-1} and 95.4 mV dec^{-1} in 0.5 M H$_2$SO$_4$ and 1 M KOH, respectively. The Tafel slopes of Co SAs/CN-1 catalyst are 288.4 and 218.6 mV dec^{-1}, respectively. The Tafel slope not only indicates that Co SAs/CN-3 catalyst has the highest efficiency of electrocatalytic hydrogen production, but also indicates that the speed control step of Co SAs/CN-3 catalyst is

Volmer step, and the electrocatalytic HER complies with Volmer–Heyrovsky mechanism.[29,30] The C_{dl} of Co SAs/CN-3 catalyst are 20.4 mF cm^{-2} in 0.5 M H$_2$SO$_4$ and 25.1 mF cm^{-2} in 1 M KOH, which is much higher than that of Co SAs/CN-1 catalyst, indicating that it has a higher electrocatalytic active surface area (Fig. S7†). Co SAs/CN-3 catalyst has the minimum impedance radius in 0.5 M H$_2$SO$_4$ (0.4 V vs. Ag/AgCl) and 1 M KOH (1.4 V vs. SCE), indicating that it has the lowest charge transfer resistance and the fastest electron transfer speed (Fig. S8†).

TOF was used to further explore the intrinsic catalytic activity of Co SAs/CN-3 catalyst. When the overpotential is 300 mV, the TOF of Co SAs/CN-3 is 0.64 s^{-1} in 0.5 M H$_2$SO$_4$, which is higher than that of Co SAs/CN-1 (~0 s^{-1}). In 1 M KOH, Co SAs/CN-3 has the highest TOF value of 0.32 s^{-1} (at 300 mV), which proves that Co SAs/CN-3 catalyst has high intrinsic activity (Fig. 3c and f). After 1000 cycles, the LSV curve in 0.5 M H$_2$SO$_4$ and 1 M KOH basically did not change, reflecting the excellent electrochemical cycling stability of Co SAs/CN-3 catalyst (Fig. 3i and j). As can be seen from the AC-HAADF-STEM image (Fig. S13†), Co atoms are still uniformly dispersed in the form of single atoms on the surface of the substrate after the stability test. After the stability test, the valence state of Co element does not change significantly, and there are still characteristic peaks at about 780.1 eV and 795.5 eV that are attributed to Co^{2+}, and the peak position is not shifted, indicating that Co SAs/CN-3 catalyst has excellent stability. After continuous testing for 20 h, the current density showed a small decrease, which further proved that the catalyst has excellent long-term stability (Fig. 3g and h).

In addition, Co SAs/CN-3 catalyst showed excellent ORR performance in 0.1 M KOH electrolyte saturated with O$_2$ (Fig. 4 and S9–S11†). LSV curve shows that the half-wave potential of Co SAs/CN-3 catalyst is 0.87 V, only 0.1 V lower than that of 20% Pt/C catalyst (0.88 V), but better than Co SAs/CN-1 (0.77 V) (Fig. 4a and c). The Tafel slope of Co SAs/CN-3 was 42.9 mV dec^{-1}, which was significantly lower than that of 20% Pt/C catalyst (59.0 mV dec^{-1}) and Co SAs/CN-1 (62.2 mV dec^{-1}) (Fig. 4b). At the potential of 0.85 V, the j_k of Co SAs/CN-3 is 8.1 mA cm^{-2}, and the j_k of Co SAs/CN-1 catalysts is 1.2 mA cm^{-2}, respectively, indicating that Co SAs/CN-3 has higher ORR catalytic efficiency (Fig. 4c and S8†). According to the K–L equation, the electron transfer number of Co SAs/CN-3 is about 4, which proves that Co SAs/CN-3 is an efficient 4-electron ORR catalytic process (Fig. 4d). RRDE test results also showed that the electron transfer number of Co SAs/CN-3 was about 4, and the hydrogen peroxide yield was almost zero, confirming again that Co SAs/CN-3 was an effective 4e$^-$ ORR catalyst (Fig. S10†). In addition, Co SAs/CN-3 showed excellent stability, with its LSV curve almost unchanged after the i–t test of 10 000 s (Fig. 4e). It can be seen from the i–t curve that the current retention rate of Co SAs/CN-3 is 77.6% after 12 h stability test (Fig. S12†). Co SAs/CN-3 also had good methanol tolerance, and it still had 87.9% current retention rate at 2000 s. However, the current density of 20% Pt/C decreased significantly after methanol was added at 500 s, and its current retention rate was only 80.7% (Fig. 4f).
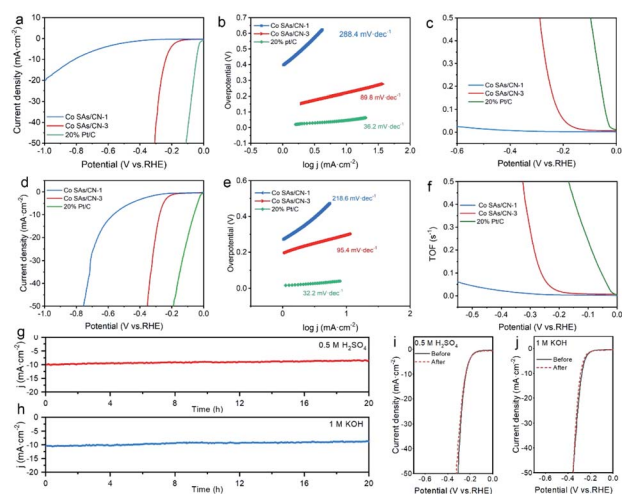

Fig. 3 Electrocatalytic HER performances. (a) LSV curves, (b) Tafel slope, (c) TOF curves, (g) i–t curve, (i) LSV curves before and after 1000 cycles in 0.5 M H$_2$SO$_4$, (d) LSV curves, (e) Tafel slope, (f) TOF curves, (h) i–t curve, (j) LSV curves before and after 1000 cycles in 1 M KOH.

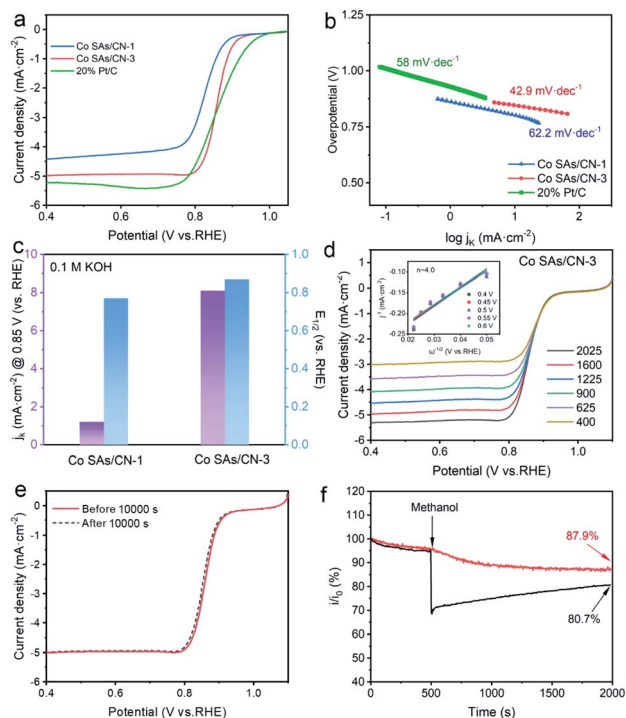© 2022 The Author(s). Published by the Royal Society of Chemistry

Fig. 4 Electrocatalytic ORR performances. (a) LSV curves, (b) Tafel slope, (c) j_k at 0.85 V and $E_{1/2}$, (d) LSV curves at different rotational speeds (insets shows the corresponding K–L plots), (e) LSV curves before and after 10 000 s, (f) methanol tolerance tests ($\sim$1.0 M methanol) in 0.1 M KOH.

Fig. 5 (a) The calculated ΔG_{H*} for different catalysts in the acidic HER process, (b) the ORR free energy diagrams in different catalysts, (c) insert image: charge density difference of Co SAs/CN-3, (d) the DOS diagrams of CoN$_4$C.

The DFT calculations were carried out to obtain a deep understanding of the excellent electrocatalytic activity of Co SAs/CN-3 catalyst. The control model of N$_4$C was built for comparison with CoN$_4$C (Fig. S14a†). For HER, the Gibbs free energy (ΔG_{H*}) of hydrogen adsorption is closer to 0 eV, indicating that the catalyst has the optimal HER catalytic activity.[31] The negative ΔG_{H*} (-1.5 eV) value of N$_4$C indicates a relatively strong hydrogen adsorption, which is not conducive to HER. The ΔG_{H*} value of Co SAs/CN-3 catalyst can be reduced to 0.1 eV (Fig. 5a), indicating that Co SAs/CN-3 is conducive for H$_2$ generation, but the adsorption ability of H* is relatively insufficient, which is consistent with the best HER catalytic activity. In other words, Co SAs/CN-3 has a more suitable ΔG_{H*} for HER. Fig. 5b shows the calculated free-energy image for 4e$^-$ reduction pathway of ORR in 0.1 M KOH. At $U = 0$ V, the free energy image of ORR over Co SAs/CN-3 catalyst showed a consistent downhill energy profile, illustrating a stable exothermal process. However, the formation of *OOH on N$_4$C is uphill in free energy. At $U = 1.23$ V, for Co SAs/CN-3 catalyst, the ΔG (1.25 eV) from *OH to OH$^-$ is the highest, indicating that it is a rate-determining step. For N$_4$C catalyst, the O$_2$ to OOH* step has the highest ΔG (1.59 eV). When CoN$_4$ is formed, there is a strong effect of electron transfer between Co and N compared with the vacancy. The electrons of nearby N will be transferred to Co to enhance the electron strength of Co surface and provide more electrons to participate in the ORR reaction (Fig. 5c). In DOS diagram (Fig. 5d and S14b†), Co SAs/CN-3 has a state at Fermi
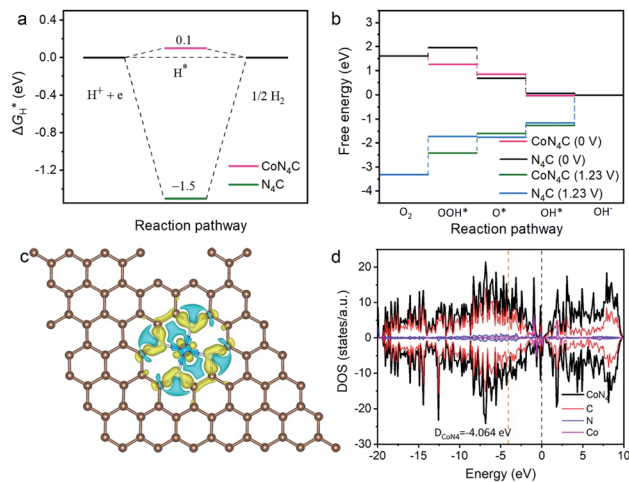
level, while N$_4$C catalyst does not exist, which indicates that the conductivity of CoN$_4$C is stronger than that of N$_4$C, and the electron transfer rate is faster. The energy band center of CoN$_4$C is closer to the Fermi level than that of N$_4$C, indicating that the surface energy is lower and the adsorption ability is stronger.[31,32] In a word, the free-energy and DOS images demonstrate that the ORR activity of Co SAs/CN-3 is superior to that of N$_4$C, which was due to the existence of the Co–N$_4$ active sites.

Conclusions

In summary, a novel doping-adsorption-pyrolysis strategy was developed for constructing carbon-supported Co single atom catalyst with a stable Co–N$_4$ coordination structure. The developed Co SAs/CN-3 catalyst showed high activity and stability for both ORR and HER due to the advantages of large specific surface area (846 m^2 g^{-1}), highly dispersed Co–N$_4$ active sites and abundant pore structure. DFT results show that the isolated active CoN$_4$ site promotes the adsorption of H and oxygen-containing intermediates in HER and ORR. This study provides a new preparation method for the design and construction of multifunctional non-precious electrocatalysts and provides a broad prospect for the wide application of renewable energy conversion equipment.

Author contributions

Yuan Pan: conceptualization, writing – review & editing, supervision, funding acquisition. Minmin Wang: methodology, investigation, data curation, writing – original draft. Chao Feng: software, methodology.

Conflicts of interest

There are no conflicts to declare.

Acknowledgements

Notes and references

1 Y. Pan, K. Sun, Y. Lin, X. Cao, Y. Cheng, S. Liu, L. Zeng, W. Cheong, D. Zhao, K. Wu, Z. Liu, Y. Liu, D. Wang, Q. Peng, C. Chen and Y. Li, *Nano Energy*, 2019, **56**, 411–419.

2 H. Wang, C. Weng and Z. Yuan, *J. Energy Chem.*, 2021, **56**, 470–485.

3 R. Zhang, A. Ma, X. Liang, L. Zhao, H. Zhao and Z. Yuan, *Front. Chem. Sci. Eng.*, 2021, **15**, 1550–1560.

4 T. Yang, C. Cui, H. Rong, J. Zhang and D. Wang, *Acta Phys.-Chim. Sin.*, 2020, **36**, 2003047.

5 Y. Li, J. He, W. Cheng, H. Su, C. Li, H. Zhang, M. Liu, W. Zhou, X. Chen and Q. Liu, *Sci. China Mater.*, 2021, **64**, 2467–2476.

6 Z. Ma, H. Tian, G. Meng, L. Peng, Y. Chen, C. Chen, Z. Chang, X. Cui, L. Wang, W. Jiang and J. Shi, *Sci. China Mater.*, 2020, **63**, 2517–2529.

7 M. Zhou, S. Bao and A. J. Bard, *J. Am. Chem. Soc.*, 2019, **141**, 7327–7332.

8 P. Jiang, H. Huang, J. Diao, S. Gong, S. Chen, J. Lu, C. Wang, Z. Sun, G. Xia, K. Yang, Y. Yang, L. Wei and Q. Chen, *Appl. Catal., B*, 2019, **258**, 117965.

9 H. Luo, Y. Liu, S. D. Dimitrov, L. Steier, S. Guo, X. Li, J. Feng, F. Xie, Y. Fang, A. Sapelkin, X. Wang and M. Titirici, *J. Mater. Chem. A*, 2020, **8**, 14690–14696.

10 Z. Liu, J. Li, S. Xue, S. Zhou, K. Qu, Y. Li and W. Cai, *J. Energy Chem.*, 2020, **47**, 317–323.

11 Y. Pan, C. Zhang, Y. Lin, Z. Liu, M. Wang and C. Chen, *Sci. China Mater.*, 2020, **63**, 921–948.

12 Y. Wang, H. Su, Y. He, L. Li, S. Zhu, H. Shen, P. Xie, X. Fu, G. Zhou, C. Feng, D. Zhao, F. Xiao, X. Zhu, Y. Zeng, M. Shao, S. Chen, G. Wu, J. Zeng and C. Wang, *Chem. Rev.*, 2020, **120**, 12217–12314.

13 A. Alarawi, V. Ramalingam and J. He, *Mater. Today Energy*, 2019, **11**, 1–23.

14 Y. Wang, F. Chu, J. Zeng, Q. Wang, T. Naren, Y. Li, Y. Cheng, Y. Lei and F. Wu, *ACS Nano*, 2021, **15**, 210–239.

15 Y. He, S. Hwang, D. A. Cullen, M. A. Uddin, L. Langhorst, B. Li, S. Karakalos, A. J. Kropf, E. C. Wegener, J. Sokolowski, M. Chen, D. Myers, D. Su, K. L. More, G. Wang, S. Litster and G. Wu, *Energy Environ. Sci.*, 2019, **12**, 250–260.

16 L. Cao, Q. Luo, W. Liu, Y. Lin, X. Liu, Y. Cao, W. Zhang, Y. Wu, J. Yang, T. Yao and S. Wei, *Nat. Catal.*, 2019, **2**, 134–141.

17 X. Liu, L. Zheng, C. Han, H. Zong, G. Yang, S. Lin, A. Kumar, A. R. Jadhav, N. Q. Tran, Y. Hwang, J. Lee, S. Vasimalla, Z. Chen, S. G. Kim and H. Lee, *Adv. Funct. Mater.*, 2021, **31**, 2100547.

18 Z. Zhang, X. Zhao, S. Xi, L. Zhang, Z. Chen, Z. Zeng, M. Huang, H. Yang, B. Liu, S. J. Pennycook and P. Chen, *Adv. Energy Mater.*, 2020, **10**, 2002896.

19 Y. Pan, R. Lin, Y. Chen, S. Liu, W. Zhu, X. Cao, W. Chen, K. Wu, W. Cheong, Y. Wang, L. Zheng, J. Luo, Y. Lin, Y. Liu, C. Liu, J. Li, Q. Lu, X. Chen, D. Wang, Q. Peng, C. Chen and Y. Li, *J. Am. Chem. Soc.*, 2018, **140**, 4218–4221.

20 Y. Pan, Y. Chen, K. Wu, Z. Chen, S. Liu, X. Cao, W. Cheong, T. Meng, J. Luo, L. Zheng, C. Liu, D. Wang, Q. Peng, J. Li and C. Chen, *Nat. Commun.*, 2019, **10**, 4290.

21 Y. Chen, S. Xu, S. Zhu, R. J. Jacob, G. Pastel, Y. Wang, Y. Li, J. Dai, F. Chen, H. Xie, B. Liu, Y. Yao, L. G. Salamanca-Riba, M. R. Zachariah, T. Li and L. Hu, *Nano Res.*, 2019, **12**, 2259–2267.

22 L. Wang, J. Zhang, L. Zheng, J. Yang, Y. Li, X. Wan, X. Liu, X. Zhang, R. Yu and J. Shui, *J. Mater. Chem. A*, 2020, **8**, 13166–13172.

23 Y. Xue, B. Huang, Y. Yi, Y. Guo, Z. Zuo, Y. Li, Z. Jia, H. Liu and Y. Li, *Nat. Commun.*, 2018, **9**, 1460.

24 W. Chen, J. Pei, C. He, J. Wan, H. Ren, Y. Zhu, Y. Wang, J. Dong, S. Tian, W. Cheong, S. Lu, L. Zheng, X. Zheng, W. Yan, Z. Zhuang, C. Chen, Q. Peng, D. Wang and Y. Li, *Angew. Chem., Int. Ed.*, 2017, **56**, 16086–16090.

25 X. Han, X. Ling, D. Yu, D. Xie, L. Li, S. Peng, C. Zhong, N. Zhao, Y. Deng and W. Hu, *Adv. Mater.*, 2019, **31**, 1905622.

26 Z. Geng, Y. Cao, W. Chen, X. Kong, Y. Liu, T. Yao and Y. Lin, *Appl. Catal., B*, 2019, **240**, 234–240.

27 T. Sun, S. Zhao, W. Chen, D. Zhai, J. Dong, Y. Wang, S. Zhang, A. Han, L. Gu, R. Yu, X. Wen, H. Ren, L. Xu, C. Chen, Q. Peng, D. Wang and Y. Li, *Proc. Natl. Acad. Sci. U. S. A.*, 2018, **115**, 12692–12697.

28 J. Yi, R. Xu, G. Chai, T. Zhang, K. Zang, B. Nan, H. Lin, Y. Liang, J. Lv, J. Luo, R. Si, Y. Huang and R. Cao, *J. Mater. Chem. A*, 2019, **7**, 1252–1259.

29 L. Zeng, K. Sun, Y. Chen, Z. Liu, Y. Chen, Y. Pan, R. Zhao, Y. Liu and C. Liu, *J. Mater. Chem. A*, 2019, **7**, 16793–16802.

30 L. Zeng, K. Sun, X. Wang, Y. Liu, Y. Pan, Z. Liu, D. Cao, Y. Song, S. Liu and C. Liu, *Nano Energy*, 2018, **51**, 26–36.

31 M. Wang, X. Zheng, D. Qin, M. Li, K. Sun, C. Liu, W. Cheong, Z. Liu, Y. Chen, S. Liu, B. Wang, Y. Li, Y. Liu, C. Liu, X. Yang, X. Feng, C. Yang, C. Chen and Y. Pan, *Small*, 2022, 2201974.

32 M. Wang, M. Li, Y. Zhao, N. Shi, H. Zhang, Y. Zhao, Y. Zhang, H. Zhang, W. Wang, K. Sun, Y. Pan, S. Liu, H. Zhu, W. Guo, Y. Li, Y. Liu and C. Liu, *J. Energy Chem.*, 2022, **67**, 147–156.